AIAA JOURNAL
Vol. 46, No. 5, May 2008

Enhanced Stability and Reduced Emissions in an Elliptic Swirl-Stabilized Burner

Christian Oliver Paschereit*
Berlin University of Technology, 10623 Berlin, Germany
and
Ephraim J. Gutmark†
University of Cincinnati, Cincinnati, Ohio 45221-0070

DOI: 10.2514/1.27872

Unstable thermoacoustic modes were studied and controlled passively by changing the geometry of a swirl-stabilized burner to an elliptic shape. The elliptic burner modified the mixing of the fuel and the air, the fresh fuel/air mixture, and the hot combustion products. The flow dynamics induced by the noncircular burner affected the flame stabilization at the central recirculation zone and at the sudden expansion. In addition to the enhanced mixing, the elliptic burner achieved lower emissions while stabilizing the combustion by reducing the coherence of the large-scale vortices at the burner's exit. The combustion tests were performed in a range of normalized equivalence ratios from near lean blowout to 1.2 times the nominal equivalence ratio, at two different power levels. In addition, power variations from 0.54 to 1.15 of the nominal power at nominal equivalence ratios were performed. Pressure and heat-release fluctuations were measured and analyzed for all operating conditions. The elliptic burner showed reductions of more than two orders of magnitude (−24 dB) in pressure and heat-release oscillations in the entire range of equivalence ratios measured. The structures of the different instability modes (axisymmetric at $St = 0.6$ and helical at 1.7 and 7.1) were studied with an intensified charge-coupled-device camera filtered to monitor OH chemiluminescence using phased-locked visualization. The axisymmetric mode showed substantially reduced variability in heat-release rate during the cycle of instability, compared with the axisymmetric baseline burner. This behavior resulted in a reduced level of instability, as evidenced from the spectral analysis of the pressure oscillations. NO_x and CO emissions were considerably reduced: NO_x by up to four times and CO by a factor of 2–3. Unburned-hydrocarbon emissions were significantly reduced for normalized equivalence ratios below 0.9, indicating an extension of the lean-blowout limit. The strong suppression of thermoacoustic instability and large reductions of emissions persisted in the entire range of power output tested.

Introduction

LARGE-SCALE coherent structures play an important role in combustion and heat-release processes by controlling the mixing between fuel and air in diffusion-flame configurations and the mixing between the fresh fuel/air mixture, hot combustion products, and fresh air in premixed combustors. The evolution of these structures in nonreacting flows was extensively studied in mixing layers (Oster and Wygnanski [1] and Ho and Huerre [2]), jets (Crow and Champagne [3] and Paschereit et al. [4]) and flows over backward-facing steps (Hasan [5]). Unlike large-scale structures in nonswirling flows, which are predominantly axisymmetric, swirl enhances azimuthal unstable modes. Interaction between large-scale structures related to flow instabilities, acoustic resonant modes in the combustion chamber, and the heat-release process was shown to cause undesired thermoacoustic instabilities in the combustor.

Swirl stabilization is used in combustion systems such as gas turbines, which also exhibit combustion instabilities. Rational modification of large-scale vortices is important to control swirl-induced instability and to increase combustion efficiency. Control of swirling flows requires an understanding of the vortical structure in this type of flow and to study the effect of forcing. The specific flow and combustion characteristics of the low-emission swirl-stabilized burner that was investigated in the present paper were described by Paschereit et al. ([6–10]). They identified the instability modes typical to this configuration and used various passive and active control methods to suppress them. The two operating modes that were studied included a partially premixed diffusion flame and premixed combustion. The diffusion flame was tuned to unstable operation with two destabilized modes: axisymmetric and helical. The premixed instability mode, which was obtained by adjusting the acoustic boundary conditions, was predominantly axisymmetric. Pressure fluctuations were detected only for the axisymmetric modes, but heat-release fluctuations, which were measured by OH chemiluminescence, indicated dual-mode behavior.

Realizing the importance of large-scale structures as drivers of combustion instabilities, researchers developed passive and active methods to control this instability by modifying the vortical structures in the flow (Schadow and Gutmark [11], McManus et al. [12], Annaswamy and Ghoniem [13], and Docquier and Candel [14]). Most of these control methods were applied to bluff-body-stabilized combustors and dump combustors in which the flow recirculation is used to stabilize the flame. Some more recent tests applied various active and passive control strategies in swirl-stabilized combustors. The present paper focuses on a passive control strategy, and some relevant literature dealing with such technology is summarized next.

The location of fuel injection in a lean premixed combustor was parametrically evaluated to determine a stable configuration (Steele et al. [15]). It was observed that small axial changes in the position of the fuel spokes within the premix duct of the fuel injector had a positive effect on decoupling the excitation of the natural acoustic modes of the combustion system. Richards and Robey [16]

Presented as Paper 1011 at the 41st AIAA Aerospace Sciences Meeting and Exhibit, Reno, NV, 6–9 January 2003; received 17 September 2006; revision received 5 July 2007; accepted for publication 6 July 2007.

*Professor, Hermann-Föttinger-Institute of Fluid Dynamics; oliver.paschereit@tu-berlin.de.

†Professor, Department of Aerospace Engineering and Engineering Mechanics; Ephraim.Gutmark@uc.edu. Senior Member AIAA.

summarized passive methods that were used to improve the stability of low-emission combustors in stationary-power gas turbines. These include the stabilizing effects of distributed time lags and of acoustic dampers. Mitchell and Karagozian [17] examined the effects of differing levels of passive fuel/air premixing on flame structures and their associated NO_x and CO emissions. Four fuel injector geometries were tested, three of which had lobed shapes. It was found that with significant air confinement, forcing more mixing between fuel and air, both NO_x and CO emissions could be simultaneously reduced.

Two passive control strategies that were successfully employed in the same burner used in the present investigation include distributed vortex generators and vortex breakdown control. Miniature vortex generators were installed at the circumference of a swirl-stabilized burner's exit to interfere with the formation of circumferential vortices through the induction of streamwise vorticity (Paschereit and Gutmark [18]). The tests showed that in addition to the effect on the initial vortices, the process that leads to the formation of large-scale vortices through pairing and vortex merging was disrupted. Thermoacoustic instabilities that are excited by the periodic heat release due to the presence of coherent vortices were thus avoided in both the high- and low-frequency ranges. The high-frequency oscillations were suppressed by up to 28 dB and low-frequency instabilities were suppressed by 50%. Emissions of NO_x were reduced by a factor of 2. Similar results were obtained in both atmospheric and high-pressure tests. Flame anchoring in a swirl-stabilized combustor occurs in an aerodynamically generated recirculation region, which is a result of vortex breakdown (VBD). Passive control of the instability was achieved by stabilizing the location of vortex breakdown using an extended lance (Paschereit et al. [19]). In addition to the passive stabilization by the extended lance, it enabled injection of secondary fuel directly into the recirculation zone in which the flame is stabilized. The VBD stabilization method has been successfully implemented in engines with sufficient stability margins and good operational flexibility.

Another approach to passive control uses noncircular geometries to enhance small-scale mixing, reduce the coherence of large-scale vortices, and generate axial vorticity. Noncircular jets have been the topic of extensive research in the last 15 years, as reviewed by Gutmark and Grinstein [20]. These jets were identified as an efficient technique of passive flow control that allows significant improvements of performance in various practical systems at a relatively low cost, because noncircular jets rely solely on changes in the geometry of the nozzle. The applications of noncircular jets include improved large- and small-scale mixing in low- and high-speed flows and enhanced combustor performance. Additional applications include noise suppression, improved heat transfer, and thrust vector control.

The flow patterns associated with noncircular jets in general, and elliptic jets in particular, involve mechanisms of vortex evolution and interaction, flow instabilities, and fine-scale turbulence augmentation (Ho and Gutmark [21] and Husain and Hussain [22]). Stability theory can be used to determine the effects of initial momentum-thickness distribution, aspect ratio, and radius of curvature on the initial flow evolution. Vortex dynamics related to self-induction and interaction between azimuthal and axial vortices lead to axis switching in the mean flowfield. These special features increase the mixing rate of such jets and produce strong azimuthal modes that reduce the vortex coherence.

The concept was first applied to elliptic swirl-stabilized burners with eccentricities of 1.18 and 1.43 by the authors at ABB Switzerland in 1997 and 1998 [23]. Polifke et al. [24] investigated three elliptical premix nozzle geometries with eccentricities of 1.5 and 2, with emphasis on time-delay impact. The nozzles produce wider time-lag distributions with smaller mean values than the circular base configuration and were therefore expected to be less prone to combustion instabilities.

The present paper describes an experimental investigation of an elliptic burner designed to suppress low- and high-frequency instability modes in the low-emission swirl-stabilized combustor. The elliptic burner was shown to be effective in suppressing different modes of thermoacoustic instabilities and, at the same time, reducing NO_x, CO, and unburned-hydrocarbon emissions in a wide range of operating conditions. The effect of the burner's geometry on the unstable modes structure and combustor performance is discussed.

Experimental Setup

Combustion Facility

The combustion facility is shown in Fig. 1. The test rig consists of a plenum chamber upstream of the swirl-inducing burner (Döbbeling et al. [25]) and a combustion chamber downstream of the burner. The plenum chamber contains perforated plates to reduce the turbulence level of the flow. The circular combustion chamber consists of an air-cooled double-walled quartz glass that provides full visual access to the flame. The exhaust system is an air-cooled tube with the same cross section as the combustion chamber, to avoid acoustic reflections at area discontinuities. The acoustic boundary conditions of the exhaust system could be adjusted from almost anechoic (reflection coefficient $|r| < 0.15$) to open-end reflection by installing an orifice plate at the exhaust with different hole diameters. The tests reported here were performed with an open Levine–Schwinger end. The flame was stabilized in a recirculation region near the burner outlet. The burner was operated at atmospheric conditions. In addition to the standard baseline round burners, an elliptic burners with an eccentricity of 1.43 was developed (Fig. 1). Because the burner is constructed from two halves of a split cone (Döbbeling et al. [26]), the elliptic burner consisted of two halves, each with a cross section of half an ellipse, with the air slots located at the major axis side.

Pressure fluctuations were measured using Brüel & Kjær water-cooled microphones. The wall-mounted water-cooled $\frac{1}{4}$-in. condenser microphones were placed at a downstream distance x, such that $x/D = 2.5$. D is defined as the major axis of the elliptic exit. The holders consisted of a small orifice ($d = 1$ mm) open to the combustion chamber. The microphone diaphragm was placed in a small cavity and was heat-radiation-protected. The resonance frequency of the holder was larger than $f_{\text{res}} > 20$ kHz. Using condenser microphones rather than piezoelectric pressure probes gave the advantage of highly accurate data in phase and amplitude, necessary for acoustic measurements. The frequency responses of the microphones in probe holders were compared against standard B&K microphones and showed good agreement. A special test rig allowed for phase and amplitude calibration of the different microphone holders. At the upper level of 142 dB, the maximum distortion was 3%. The averaging of the frequency spectra was performed using $\mathrm{d}f = 2.93$ Hz. A low-pass filter of 10 kHz was used.

The operating conditions of the burner were maintained by analyzing the exhaust gas composition using a physical gas analysis system. CO and CO_2 were analyzed by using nondispersive infrared spectroscopy (linearity error of 1% and repetition precision of 0.5%). The nitric oxides NO and NO_2, combined in NO_x, were detected with a chemiluminescence analyzer (linearity error of 1% and repetition precision of 0.25%). The detection of the remaining O_2 in the exhaust gas was made using the paramagnetic properties of oxygen in the analyzing device (linearity error of 0.5% and repetition precision of 0.5%). Carbon and oxygen balances were continuously computed, and agreement within 0.2% was assured. Overall accuracy of the emissions measurements was within 2%. The fuel flow rate was measured using Coriolis mass flow meters with an accuracy of 0.6–2% for flow rates between 20 to 1.5 kg/h, respectively. The airflow rate was measured with an accuracy of 3%. The equivalence ratio was determined with an accuracy of 5%.

The tests included flame-temperature variations from 20% above nominal to the lean blowout (LBO) limit, at a nominal power and at 68% of the nominal power. The latter test was performed to maintain the same pressure drop in the elliptic burner as in the circular burner, which had a larger exit area. In addition, normalized power variations from 54 to 115% of the nominal power level, at nominal flame temperature, were performed. Because of proprietary considerations, all quantities were normalized by their values for the circular burner at the nominal power and nominal equivalence ratio.

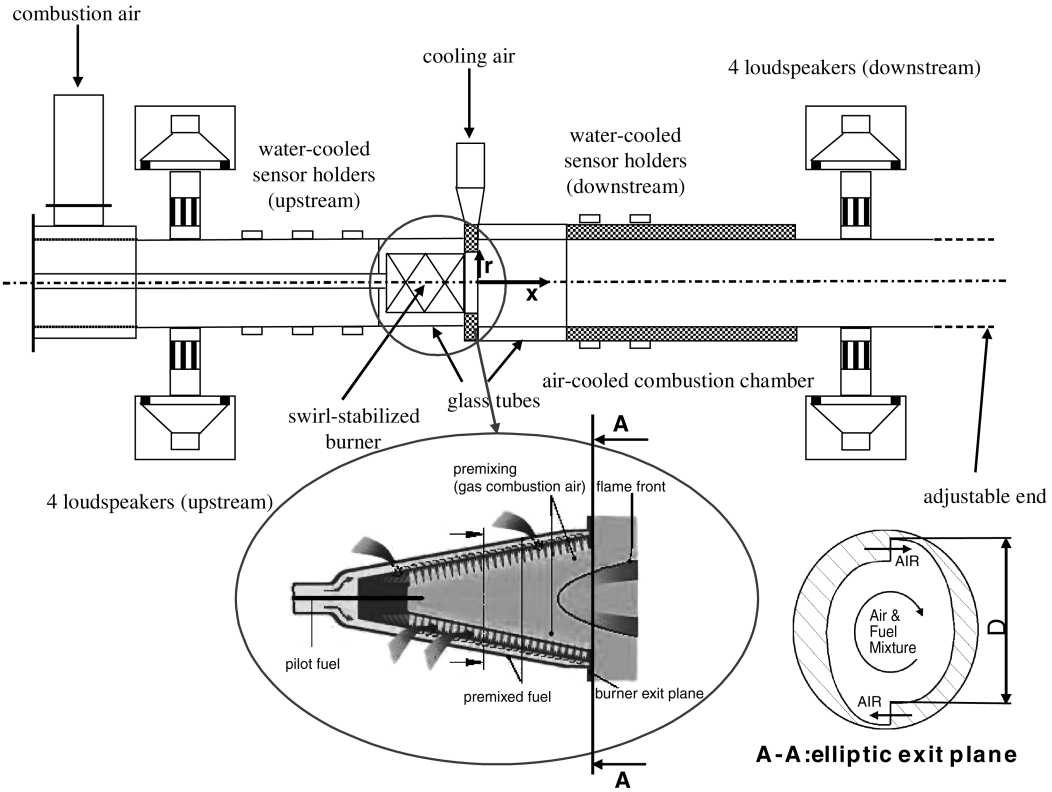

Fig. 1 Experimental arrangement of the combustor; the insert on the right displays the elliptic burner exit cross section.

Heat-Release Measurements and Visualization System

Time-varying heat release was recorded with two filtered fiber-optic probes to detect OH radiation. Several studies have shown that OH appears in superequilibrium concentrations in the flame-front region (Cattolica [27]). Therefore, the OH emissions were used as a qualitative indicator to detect the heat release at the active combustion regions. The signal was bandpass-filtered with a lower and higher cutoff wavelength of 290 and 390 nm, respectively. The circular field of view of the probes had a diameter of $d = 10$ mm at the flame position. The probe was coupled with a photomultiplier with a response time of 1 ns. The probe monitored the upper shear layer ($r/D = 0.5$) at a position of $x/D = 0.5$ downstream from the dump plane. A bandpass filter between 290 and 390 nm was deployed.

Phase-locked pictures of the flame were obtained using an amplified (microchannel plate) CCD camera with an exposure time of 20 μs. The camera was triggered by the pressure signals, which were bandpass-filtered at the instability frequency and phase-shifted. The images were filtered using a bandpass filter with low and high cutoff wavelengths of 29 and 390 nm, respectively. The phase-locked exposures were then averaged over 64 events.

Results and Discussion

Combustion Dynamics: Pressure and Heat Release

Thermoacoustic instabilities could be excited in the circular combustor by proper adjustment of the acoustic boundary conditions. The source and structure of these instabilities were described by Paschereit et al. [6]. The frequency and intensity of the unstable modes were recorded from pressure and OH chemiluminescence oscillations (integrated along a line of sight across the combustor at $x/D = 0.5$ cm from the burner exit). The baseline circular burner produced an axisymmetric dominant unstable mode at $St = 0.6$ and two smaller helical modes: one at $St = 1.1$ and another low-amplitude mode at $St = 7.2$ (Fig. 2). The pressure oscillations were normalized by their level in a circular nozzle at nominal power and nominal stoichiometric conditions, and the St is the normalized frequency, defined as $St = fD/U$, where U is the mean velocity at the burner's exit. The pressure fluctuations were strongest at $St = 0.6$. The high-frequency peak was observed to increase and become dominant at higher burner power.

These three unstable modes appear both in the pressure and OH-chemiluminescence spectra. Some heat-release modes that were identified in the OH spectra did not couple with the acoustic modes and did not excite thermoacoustic pressure modes. The two peak frequencies of the OH fluctuations in this case were at $St = 0.6$ and $St = 1.1$, and the pressure fluctuations were strongest at $St = 0.6$. The lower-frequency instability was identified elsewhere (Paschereit et al. [6]) as an axisymmetric instability, and the higher-frequency instability was helical.

The structure of the three different instability modes of the baseline circular burner ($St = 0.6, 1.1, 7.2$) was studied with a CCD

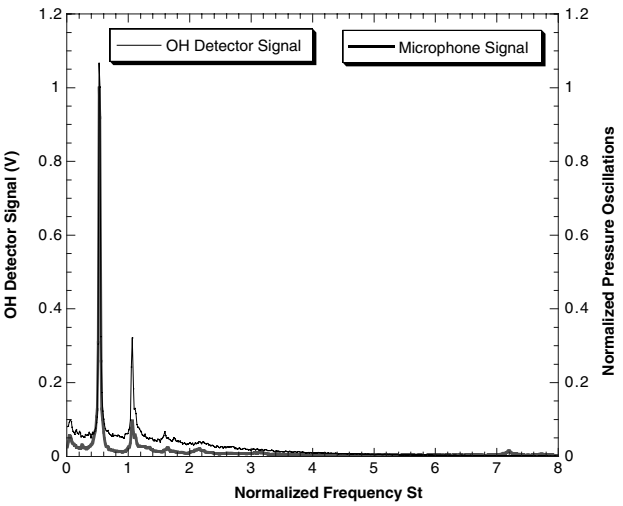

Fig. 2 Pressure and OH-chemiluminescence spectra during unstable operation of the baseline circular burner; nominal power and equivalence ratio; pressure is measured on the combustor wall at $x/D = 2.5$ and OH is measured at $r/D = 0.5$ and $x/D = 0.5$.

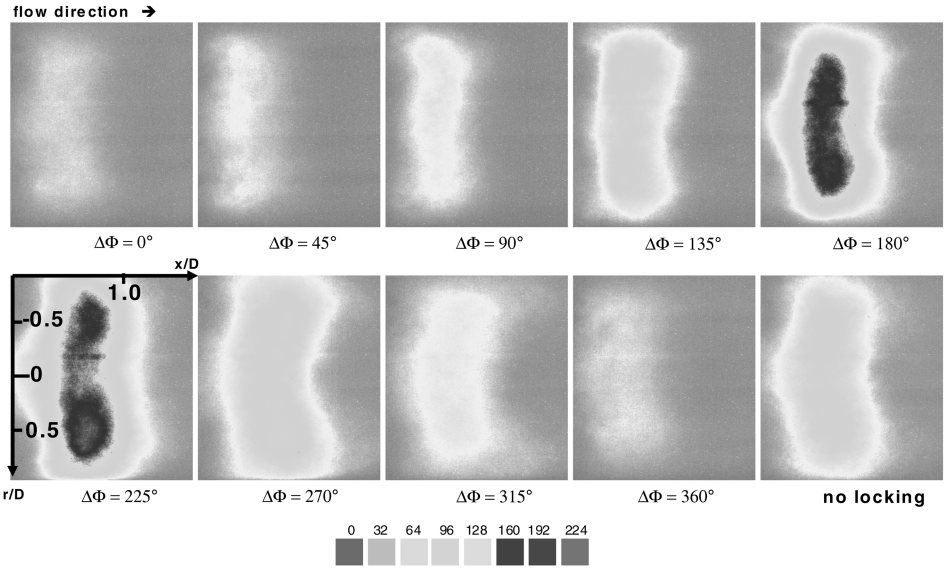

Fig. 3 OH-Chemiluminescence phase-locked visualizations of the axisymmetric low-frequency ($St = 0.6$) instability of the circular burner; arbitrary phases are referenced to the first frame shown; nominal power and equivalence ratio.

camera filtered to monitor OH chemiluminescence using phased-locked visualization. The main high-amplitude instability at $St = 0.6$ is displayed in Fig. 3. The phase angles of the different frames are arbitrary and referenced to the first frame in the figure. Strong variations in the heat release were observed during one cycle of instability, while maintaining the axisymmetric structure.

The elliptic burner, operating at the same conditions, had a significant impact on the thermoacoustic instabilities both in frequency and intensity. The spectra of the pressure and OH fluctuations in the burner's shear layer and on the centerline in the elliptic burner are shown in Fig. 4. The measurements were performed at nominal power and equivalence ratio. The shear-layer OH spectrum shows a strong instability mode at a frequency of $St = 1.7$ and a weaker one at $St = 0.6$, whereas the OH spectrum measured along the centerline shows strong peaks at both frequencies. The pressure spectrum shows high amplitude at $St = 0.6$ and a very low peak at the $St = 1.7$. A small pressure peak is also visible at the high frequency of $St = 7.1$. From radial cross-correlation data discussed in the following sections, the $St = 0.6$ peak was identified as an axisymmetric instability, whereas the $St = 1.7$ peak was a helical instability. The level of the peak pressure fluctuations in the elliptic burner was more than an order of magnitude lower than that of the circular burner.

The intensity of the thermoacoustic instability, as reflected by the amplitude of the pressure and heat-release (OH chemiluminescence) fluctuations, changed as a function of operating conditions such as the flame temperature (related to the equivalence ratio) and the power output. The baseline pressure-amplitude peaks near the nominal flame temperature and is lower for leaner and richer mixtures (Fig. 5). The pressure-oscillation amplitude was normalized with the level at the nominal equivalence ratio (i.e., at a normalized equivalence ratio of 1) and nominal power. The elliptic burner was compared with the circular burner at the nominal power and at a reduced-power level (32% lower than nominal power). The reason for operating the burner at the reduced power was to yield the same pressure drop as the circular burner. The elliptic burner was formed by placing

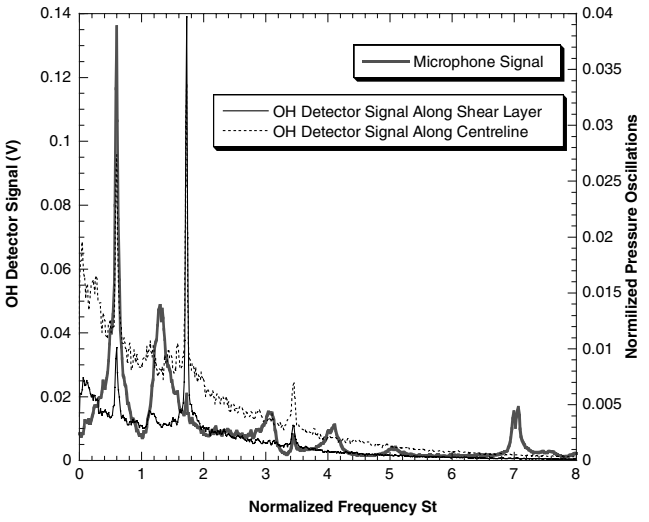

Fig. 4 Pressure and OH-chemiluminescence spectra for the elliptic burner measured on the shear layer and centerline; pressure is measured on the combustor wall at $x/D = 2.5$, shear layer OH is measured at $r/D = 0.5$ and $x/D = 0.5$, and centerline OH is measured at $r/D = 0$ and $x/D = 0.5$; nominal power and equivalence ratio.

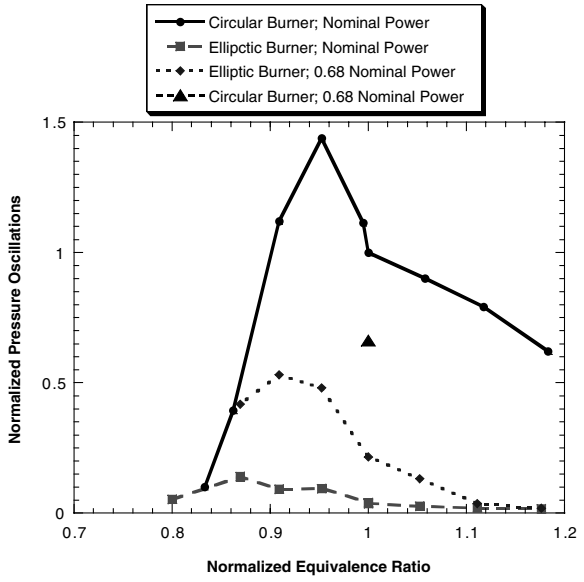

Fig. 5 Circular and elliptic burners pressure fluctuation for a range of equivalence ratios at two power levels measured on the combustor wall at $x/D = 2.5$.

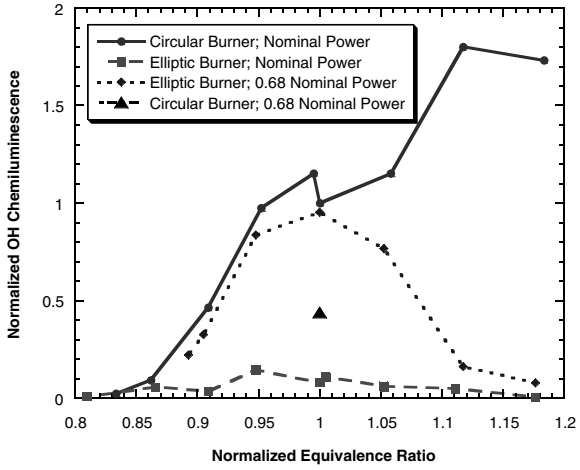

Fig. 6 Circular and elliptic burners' OH-chemiluminescence fluctuations for a range of equivalence ratios at two power levels; OH is measured at $r/D = 0.5, x/D = 0.5$.

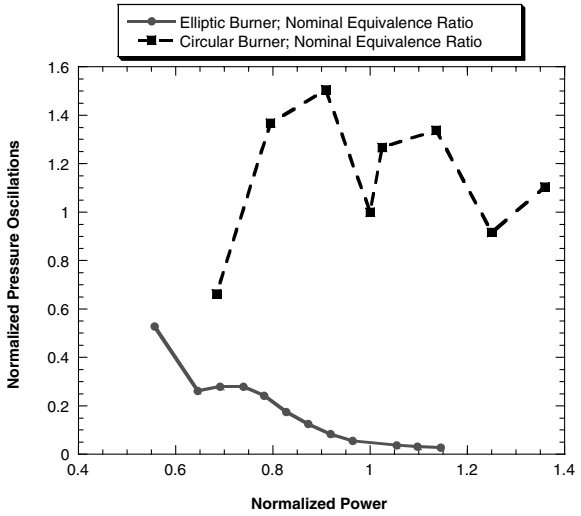

Fig. 7 Circular and elliptic burners' pressure fluctuation as a function of power at the nominal equivalence ratio; measured on the combustor wall at $x/D = 2.5$.

elliptical inserts into the circular burner, resulting in a change in the pressure drop across the burner. The reduced power enabled comparison at the same pressure drop level. The baseline pressure-pulsation level of the circular burner at the nominal equivalence ratio and at reduced power (68% of nominal) is also given in Fig. 5. At this power level, the instability was reduced by factors of nearly 3 and 4 at the nominal flame-temperature conditions relative to the baseline burner at reduced and full power, respectively. The elliptic nozzle yielded reduction of more than an order of magnitude (−24 dB in some cases) in pressure oscillations in the entire range of flame temperatures, except near the LBO limit (Fig. 5). A small extension of the LBO limit was also observed. The normalized OH-chemiluminescence fluctuations (normalized by their level at nominal power and equivalence ratio) are shown as a function of flame temperature in Fig. 6. The amplitude of the OH chemiluminescence was an order of magnitude lower than the circular burner in most of the flame-temperature range, except near the LBO limit. However, the comparison with the reduced-power baseline burner showed increased fluctuations at the nominal equivalence ratio. Because the OH measurements are monitoring one location within the combustion zone, such changes could also be related to changes in the flame-front location. The OH-chemiluminescence fluctuations at the reduced-power condition were lower for flame temperatures below the nominal level.

Figure 7 shows the behavior of the elliptic burner in a wide range of power variation compared with the circular burner. The strong suppression of thermoacoustic instability persisted in the entire range of power output tested. The suppression became more effective at high power levels. At power levels higher than 14% above the nominal level, the high-frequency instability at $St = 7.1$ was dominant.

Structure of the Instability

Phase-Locked OH Visualizations and Pressure and OH Spectra

The structure of the axisymmetric instability mode of the elliptic burner at $St = 0.6$ was studied by phased-locked visualization acquired with an ICCD camera, which was filtered to monitor OH chemiluminescence (Fig. 8). The images in Fig. 8 show a symmetric structure with varying intensity during the cycle. The maximum intensity occurred at a phase angle of 315 deg and the lowest intensity was at 135 deg. This periodic variation of OH chemiluminescence during one cycle of instability was emphasized by integrating the intensity over the entire flame at each phase angle and plotting it (arbitrary grayscale levels) as a function of that phase angle (Fig. 9). The integration was done in three steps: integration of the lower and upper halves of the flame separately and then a sum of the two. The axisymmetric mode showed substantially reduced variability in the heat-release rate during one cycle, compared with the axisymmetric instability mode in the baseline circular burner (Figs. 3 and 10).

This behavior resulted in a reduced level of instability, as evidenced in the lower pressure-oscillation peak level in the spectral

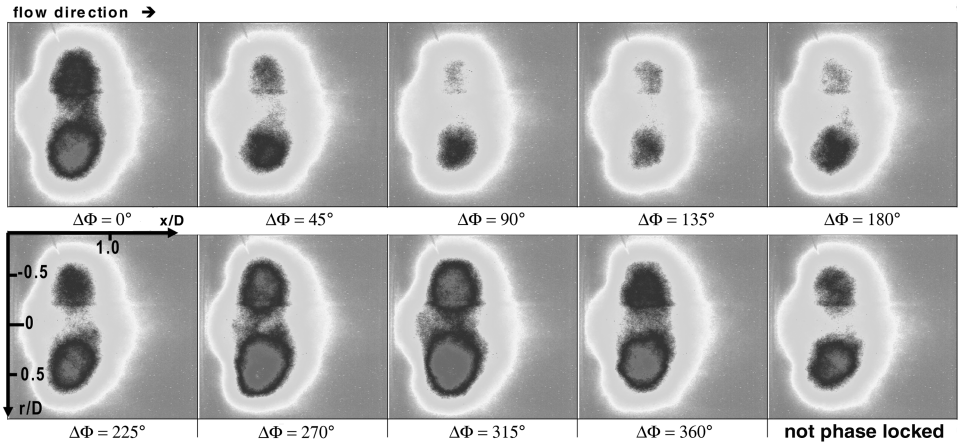

Fig. 8 OH-chemiluminescence phase-locked visualizations of the axisymmetric instability mode at $St = 0.6$ of the elliptic burner; arbitrary phases are referenced to the first frame shown; nominal power and equivalence ratio.

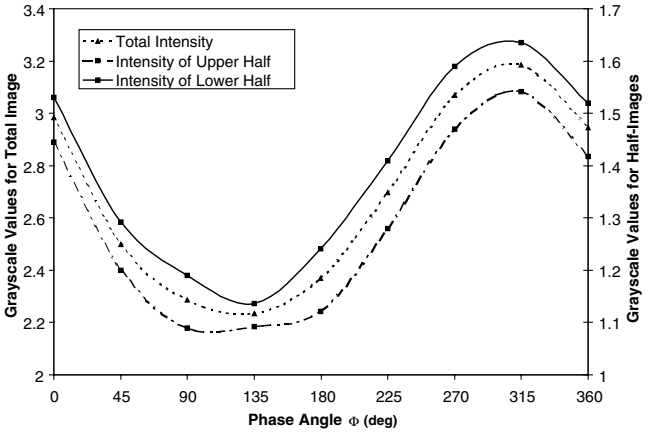

Fig. 9 Integrated OH-chemiluminescence over the upper and lower halves of the elliptic burner's flame and over the entire flame for the axisymmetric $St = 0.6$ instability.

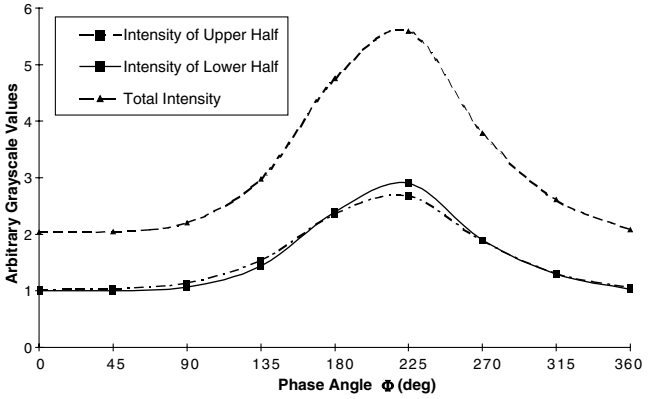

Fig. 10 Integrated OH-chemiluminescence over the upper and lower halves of the circular burner's flame and over the entire flame for the axisymmetric $St = 0.6$ instability.

plots (Fig. 4), when compared with the baseline circular burner (Fig. 2). The helical nature of the higher-frequency instabilities at $St = 1.7$ and 7.7 resulted in a change in the location of maximum heat release between the upper and lower halves of the flame, rather than the axisymmetric cyclical changes of heat release during a period of instability (Paschereit et al. [6]).

Cross-Correlations

The structure of the different instability modes was determined from radial and axial cross-correlations of OH-chemiluminescence signals measured by filtered fiber-optic probes. In the radial cross-correlation measurements, both probes were located at an axial distance of $x/D = 0.37$ from the burner's exit plane. The axial cross-correlations were measured along the combustor centerline and along its shear layer. The position of one probe was fixed at an axial distance of $x/D = 0.086$ from the burner's exit, and the other probe was moved gradually downstream (increasing the distance between them, Δx), keeping its radial location constant.

The phase and coherence of the radial cross-correlations measurements were measured for the low-frequency instabilities: $St = 0.6$ for the circular and elliptic burners and $St = 1.7$ for the elliptic burner. The measurements were performed at nominal power and flame temperature. The phase change across the combustor at various nondimensional radial distance $\Delta r/R$ (where $R = D/2$ and Δr is the distance between the probes) shows that the $St = 0.6$ instability was axisymmetric, with no radial phase change in both the circular and elliptic burners, whereas the $St = 1.7$ mode was helical, as indicated by a phase change of 140 deg (Fig. 11).

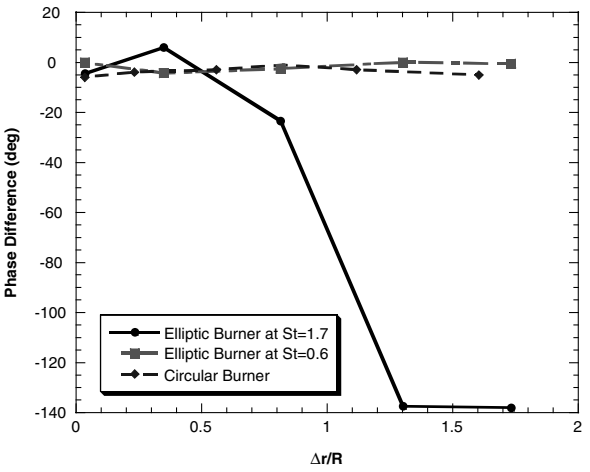

Fig. 11 Radial cross-correlation phase-difference variation with radial distance across the burner flame for the circular and elliptic burners; both probes are at $x/D = 0.37$, with the stationary probe at $r/D = 0.5$.

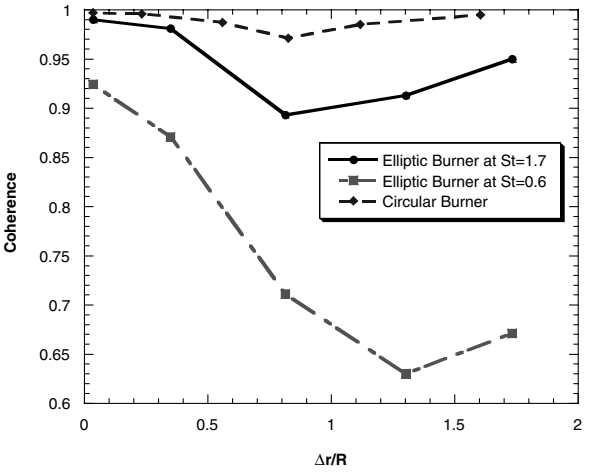

Fig. 12 Radial cross-correlation coherence variation with radial distance across the burner flame for the circular and elliptic burners; both probes are at $x/D = 0.37$, with the stationary probe at $r/D = 0.5$.

The suppression of the instability by the elliptic burner is reflected in the reduced coherence across the combustor in the radial direction, when compared with the circular burner. The coherence of the axisymmetric instability for the elliptic burner is less than 0.65, compared with nearly one for the plain burner (Fig. 12). The helical instability of the elliptic burner has a higher coherence of 0.9 than the axisymmetric mode, indicating that this mode is the dominant one. This mode is associated with the helical flow instability, but is harmless in the combustor, because it excites only evanescent acoustic modes.

The coherence of the axial cross-correlations along the centerline is shown in Fig. 13. Those along the shear layer are displayed in Fig. 14. The axial cross-correlations were measured for the axisymmetric mode at $St = 0.6$ only. The cross-correlations are calculated from the two OH probes that integrate over a line of sight; they are not at the same location for $x/D = 0$, due to their finite size, and they are neither precisely aligned nor do they provide point measurements. In addition, the accuracy of the coherence is estimated to be within 15% of the value shown, and therefore the coherence level is not 1 for $x/D = 0$. However, the large differences between the circular and elliptic burners can still be assessed. The coherence of the cross-correlation along the shear layer decays faster than that along the centerline, indicating that the large-scale structures in the shear layer of the elliptic burner lose their coherence within one diameter distance from the burner's exit. The coherence of the cross-correlations along the centerline is initially higher for

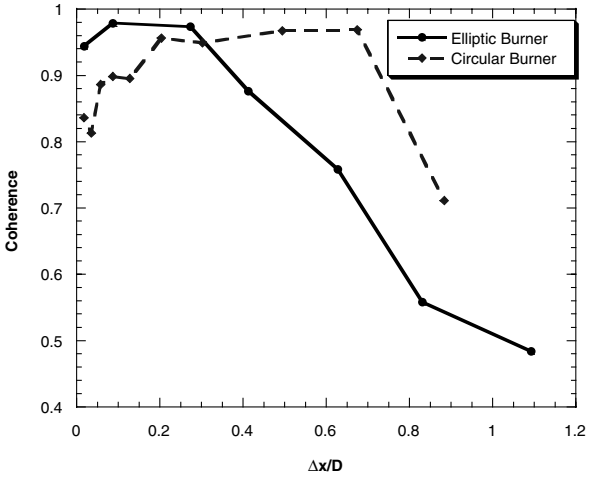

Fig. 13 Axial cross-correlation coherence variation with axial distance along the centerline of the circular and elliptic burners; both probes are at $r/D = 0$, with the stationary probe at $x/D = 0.086$.

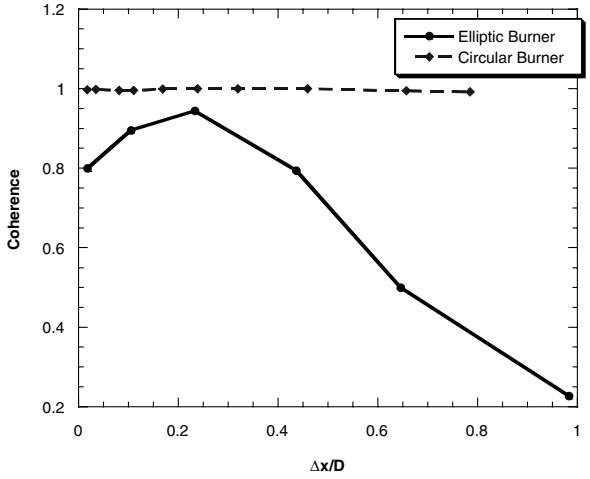

Fig. 14 Axial cross-correlation coherence variation with axial distance along the shear layer of the circular and elliptic burners; both probes are at $r/D = 0.5$, with the stationary probe at $x/D = 0.086$.

the elliptic burner but decays rapidly in axial distance, when compared with the circular burner, indicating that the heat release loses its coherence faster in the elliptic burner. In the shear layer, the coherence of the circular burner was high in the entire measurement domain and was always smaller for the elliptic burner.

Effect on Emissions

The NO_x and CO emissions from the circular and elliptic burners were measured in a wide range of flame temperatures and power outputs. The NO_x emissions were measured at nominal power for the circular and elliptic burners and at a reduced power for the elliptic burner, for comparison with the circular burner at equal pressure drop (Fig. 15). The NO_x emissions increased in both burners with the flame temperature (or equivalence ratio). The NO_x emissions were reduced by 30–40% for the same power and by about 50% at the reduced power. CO was decreased in the entire range of flame temperatures, but especially at flame temperature below the nominal level (Fig. 16). The delayed increase in CO level was indicative of an extended LBO limit.

The emissions tests were repeated at the nominal flame temperature for a range of power output. The NO_x was decreased in the entire range by a factor of more than four (Fig. 17), and the CO was decreased by 30–40% (Fig. 18).

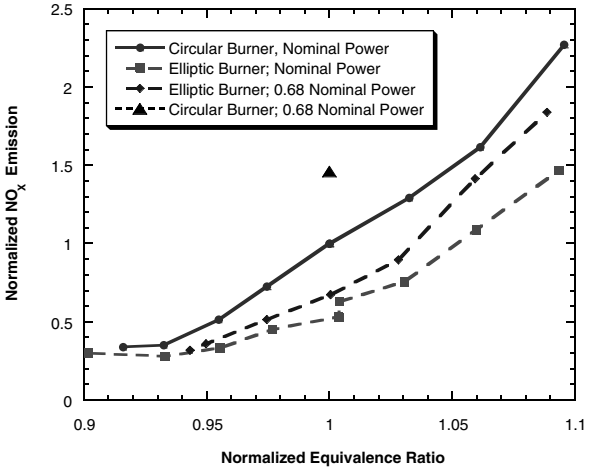

Fig. 15 NO*x* emission (based on 15% O_2) variation with equivalence ratio at two power levels for the circular and elliptic burners.

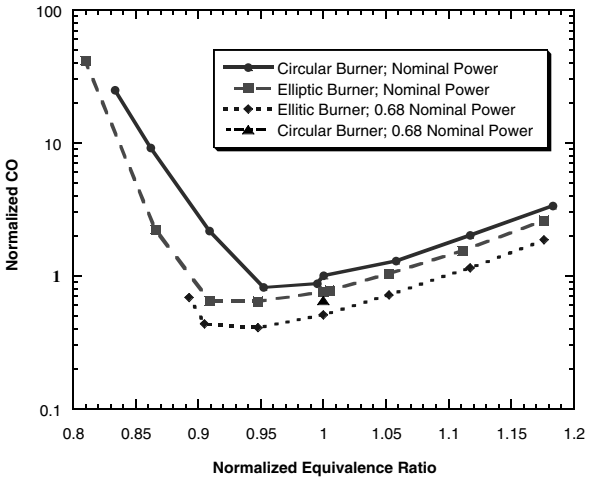

Fig. 16 CO emission (based on 15% O_2) variation with equivalence ratio at two power levels for the circular and elliptic burners.

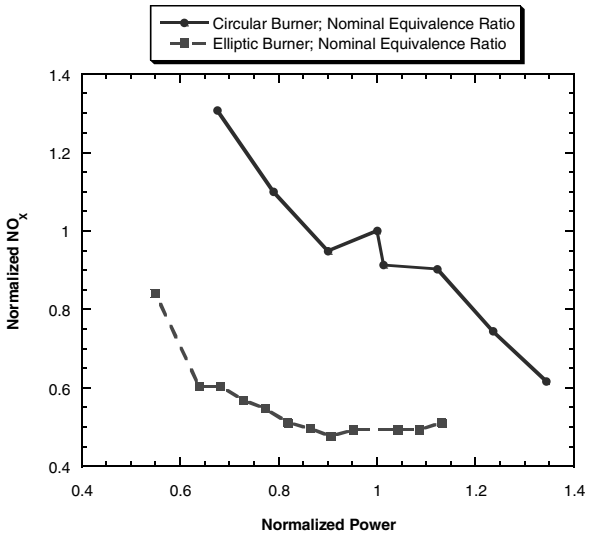

Fig. 17 NO_x emission (based on 15% O_2) variation with power at the nominal equivalence ratio for the circular and elliptic burners.

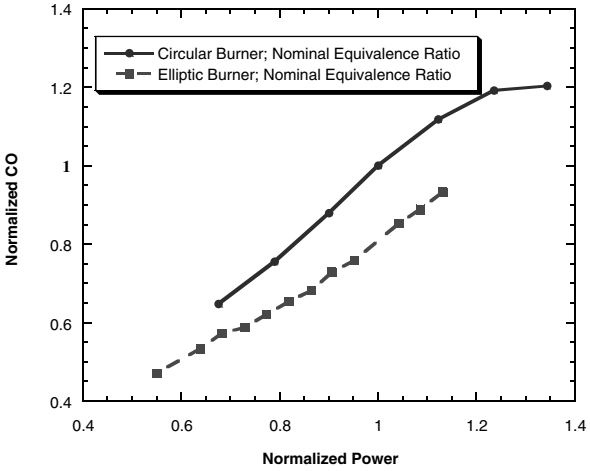

Fig. 18 CO emission (based on 15% O_2) variation with power at the nominal equivalence ratio for the circular and elliptic burners.

Conclusions

A elliptic swirl-inducing burner was designed as a passive control means to suppress unstable thermoacoustic modes in a low-emission swirl-stabilized experimental burner. Both axisymmetric and helical unstable modes were identified. Helical instability modes were excited by flow instabilities in the wakelike region at the combustor axis caused by vortex breakdown. Axisymmetric modes were associated with the shear-layer instabilities at the sudden expansion (dump plane). The elliptic burner modified the mixing between the fuel and the air and between the fresh fuel/air mixture and the hot combustion products in the recirculation zones due to its geometry. The elongated shape of the burner modified the dynamics of the vortices within the shear layers, leading to vortex bending, self-induction, and vortex interactions. These special dynamics significantly increased the mixing rate induced by the elliptic burner and produced strong azimuthal modes, thereby reducing the coherence of the vortices exiting the burner. The modified flowfield affected the flame stabilization at the central recirculation zone and at the sudden expansion. In addition to the enhanced mixing, the burner achieved reduced NO_x and CO emissions and strengthened the combustion stabilizing mechanism. The combustion tests were performed in a range of normalized equivalence ratio (flame temperature) from near LBO to 1.2 times the nominal equivalence ratio, at two different power levels. In addition, power variations from 0.54 to 1.15 of the nominal power at the nominal equivalence ratio were performed. Pressure and heat-release fluctuations were measured and analyzed at all of the operating conditions previously mentioned. The elliptic nozzle showed reductions of more than two orders of magnitude (−24 dB) in pressure and heat-release oscillations in the entire range of equivalence ratios measured. The structures of the different instability modes (axisymmetric at $St = 0.6$ and helical at 1.7 and 7.1) were studied with an ICCD camera filtered to monitor OH chemiluminescence using phased-locked visualization. The axisymmetric mode showed substantially reduced variability in the heat-release rate during a cycle of instability, compared with the circular burner axisymmetric instability mode. This behavior resulted in a reduced level of instability, as evidenced from the spectral analysis of the pressure oscillations. NO_x and CO emissions were considerably reduced: NO_x by up to four times and CO by a factor of 20–33%. The strong suppression of thermoacoustic instability and large reductions of emissions persisted in the entire range of flame temperature and power output tested.

References

[1] Oster, D., and Wygnanski, I., "The Forced Mixing Layer Between Parallel Streams," *Journal of Fluid Mechanics*, Vol. 123, 1982, pp. 91–130.
doi:10.1017/S0022112082002973

[2] Ho, C., and Huerre, P., "Perturbed Free Shear Layers," *Annual Review of Fluid Mechanics*, Vol. 16, 1984, pp. 365–424.
doi:10.1146/annurev.fl.16.010184.002053

[3] Crow, S., and Champagne, F., "Orderly Structure in Jet Turbulence," *Journal of Fluid Mechanics*, Vol. 48, 1971, pp. 547–591.
doi:10.1017/S0022112071001745

[4] Paschereit, C. O., Wygnanski, I., and Fiedler, H. E., "Experimental Investigation of Subharmonic Resonance in an Axisymmetric Jet," *Journal of Fluid Mechanics*, Vol. 283, 1995, pp. 365–407.
doi:10.1017/S0022112095002369

[5] Hasan, M. A. A., "The Flow over a Backward-Facing Step Under Controlled Perturbation: Laminar Separation," *Journal of Fluid Mechanics*, Vol. 238, 1992, pp. 73–96.
doi:10.1017/S0022112092001642

[6] Paschereit, C. O., Gutmark, E., and Weisenstein, W., "Structure and Control of Thermoacoustic Instabilities in a Gas-Turbine Combustor," *Combustion Science and Technology*, Vol. 138, Nos. 1–6, Sept. 1998, pp. 213–232.
doi:10.1080/00102209808952069

[7] Paschereit, C. O., Gutmark, E., and Weisenstein, W., "Control of Thermoacoustic Instabilities and Emissions in an Industrial-Type Gas-Turbine Combustor," *Twenty-Seventh Symposium (International) on Combustion*, Vol. 27, Combustion Inst., Pittsburgh, PA, 1998, pp. 1817–1824.

[8] Paschereit, C. O., Gutmark, E., and Weisenstein, W., "Suppression of Combustion Instabilities by Acoustic Control of Shear Layer Properties," *Advances in Turbulence*, edited by U. Frisch, Kluwer Academic, Boston, 1998, pp. 293–296.

[9] Paschereit, C. O., Gutmark, E., and Weisenstein, W., "Coherent Structures in Swirling Flows and Their Role in Acoustic Combustion Control," *Physics of Fluids*, Vol. 11, No. 9, 1999, pp. 2667–2678.
doi:10.1063/1.870128

[10] Paschereit, C. O., Gutmark, E., and Weisenstein, W., "Excitation of Thermoacoustic by the Interaction of Acoustics and Unstable Swirling Flow," *AIAA Journal*, Vol. 38, No. 6, June 2000, pp. 1025–1034.

[11] Schadow, K. C., and Gutmark, E., "Combustion Instability Related to Vortex Shedding in Dump Combustors and Their Passive Control," *Progress in Energy and Combustion Science*, Vol. 18, No. 2, 1992, pp. 117–132.
doi:10.1016/0360-1285(92)90020-2

[12] McManus, K. R., Poinsot, T., and Candel, S. M., "A Review of Active Control of Combustion Instabilities," *Progress in Energy and Combustion Science*, Vol. 19, No. 1, Feb. 1993, pp. 1–29.
doi:10.1016/0360-1285(93)90020-F

[13] Annaswamy, A. M., and Ghoniem, A. F., "Active Control in Combustion Systems," *IEEE Control Systems Magazine*, Vol. 15, No. 6, Dec. 1995, pp. 49–63.
doi:10.1109/37.476386

[14] Docquier, N., and Candel, S., "Combustion Control and Sensors: A Review," *Progress in Energy and Combustion Science*, Vol. 28, No. 2, 2002, pp. 107–150.
doi:10.1016/S0360-1285(01)00009-0

[15] Steele, R. C., Cowell, L. H., Cannon, S. M., and Smith, C. E., "Passive Control of Combustion Instability in Lean Premixed Combustors," *Journal of Engineering for Gas Turbines and Power*, Vol. 122, No. 3, July 2000, pp. 412–419.
doi:10.1115/1.1287166

[16] Richards, G. A., Straub, D. L., and Robey, E. H., "Passive Control of Combustion Dynamics in Stationary Gas Turbines," *Journal of Propulsion and Power*, Vol. 19, No. 5, 2003, pp. 795–810.

[17] Mitchell, M. G., Smith, O. I., and Karagozian, A. R., "Passive Fuel-Air Mixing and Emissions Control via Lobed Injectors," *AIAA Journal*, Vol. 42, No. 1, 2004, pp. 61–69.

[18] Paschereit, C., and Gutmark, E., "Control of High Frequency Thermoacoustic Pulsations by Distributed Vortex Generators," *AIAA Journal*, Vol. 44, No. 3, Mar. 2006, pp. 550–557.

[19] Paschereit, C., Flohr, P., and Gutmark, E., "Combustion Control by Vortex Breakdown Stabilization," *Journal of Turbomachinery*, Vol. 128, No. 4, Oct. 2006, pp. 679–688.
doi:10.1115/1.2218521

[20] Gutmark, E., and Grinstein, F., "Mixing in Non-Circular Jets," *Annual Review of Fluid Mechanics*, Vol. 31, 1999, pp. 239–272.
doi:10.1146/annurev.fluid.31.1.239

[21] Ho, C. M., and Gutmark, E., "Vortex Interaction and Mass Entrainment in a Small Aspect Ratio Elliptic Jet," *Journal of Fluid Mechanics*, Vol. 179, 1987, pp. 383–405.
doi:10.1017/S0022112087001587

[22] Husain, H. S., and Hussain, F., "Elliptic Jets, Part 1: Characteristics of Unexcited and Excited Jets," *Journal of Fluid Mechanics*, Vol. 208, 1989, pp. 257–320. doi:10.1017/S0022112089002843

[23] Paschereit, C. O., and Gutmark, E., "Brenner," ABB Switzerland Ltd., European Patent EP 0 985 876 A1, 1998.

[24] Polifke, W., Kopitz, J., and Serbanovic, A., "Impact of the Fuel Time Lag Distribution in Elliptical Premix Nozzles on Combustion Stability," 7th AIAA/CEAS Aeroacoustics Conference, Maastricht, The Netherlands, AIAA Paper 2001-2104, 28–30 May 2001.

[25] Döbbeling, K., Knöpfel, H. P., Polifke, W., Winkler, D., Steinbach, C., and Sattelmayer, T., "Low NO_X Premixed Combustion of MBTU Fuels Using the ABB Double Cone Burner (EV Burner)," American Society of Mechanical Engineers Paper 94-GT-394, 1994.

[26] Döbbeling, K., Eroglu, A., Joos, F., and Hellat, J., "Novel Technologies for Natural Gas Combustion in Turbine Systems," *Eurogas '99*, Ruhr Univ., Bochum, Germany, 25–27 May 1999.

[27] Cattolica, R. J., "OH Radical Nonequilibrium in Methane-Air Flat Flames," *Combustion and Flame*, Vol. 44, Jan. 1982, pp. 43–59. doi:10.1016/0010-2180(82)90062-1

T. Jackson
Associate Editor